

Bandstructure Effects in Phosphorene Nanoribbon MOSFETs from NEGF Simulations Using a New DFT-based Tight-binding Hamiltonian Model

Mirko Poljak* and Mislav Matic
Computational Nanoelectronics Group
University of Zagreb, Faculty of Electrical Engineering and Computing
Zagreb, HR 10000, Croatia
*Corresponding author: mirko.poljak@fer.hr

Abstract—Electronic and transport properties of monolayer black phosphorus (phosphorene) make it promising for future nanoscale field-effect transistors (FETs), especially in the form of phosphorene nanoribbons (PNRs). Currently, these devices can be explored appropriately only by means of advanced formalisms such as quantum transport that accounts for atomically-resolved description of the system under study. In this work we report a new tight-binding (TB) model for phosphorene calibrated on *ab initio* density-functional theory (DFT) calculations that accurately reproduces the bandstructure of PNRs with the widths down to ~0.5 nm. The new DFT-TB Hamiltonian produces qualitatively and quantitatively different results in terms of PNR FET performance in comparison to the widely used TB model from the literature. We show that PNR FETs with nanoribbon widths larger than ~1.4 nm can meet industry requirements at the "3 nm" node assuming ballistic transport.

Keywords—phosphorene, black phosphorus, nanoribbon, DFT, tight-binding, bandstructure, quantum transport, NEGF, MOSFET

I. INTRODUCTION

Among 2D materials (2DM) discovered after graphene [1], monolayer black phosphorus (phosphorene) is often identified as a promising contender for 2DM-based electron devices due to its appropriate bandgap value and relatively high carrier mobility, especially in comparison to transition-metal dichalcogenides such as MoS₂ [2]–[4]. While microscale phosphorene field-effect transistors (FETs) have been experimentally demonstrated [3], [5], [6], nanostructures such as phosphorene nanoribbons (PNRs) [7]–[9] are most likely needed for ultra-high density integration on chip. Due to their small dimensions along at least one direction, PNRs experience quantum effects that severely impact their electronic, transport and device properties [10]–[12].

Advanced formalisms such as atomistic non-equilibrium Green's function (NEGF) formalism are needed to predict the performance of PNR FETs, which in turn demands accurate but numerically efficient device Hamiltonians. A tight-binding (TB) model for phosphorene described in [13] is widely used in the literature to study both the material and device properties [11], [14]–[16]. However, this TB model does not reproduce the

bandstructure of sub-5 nm-wide PNRs well in comparison to *ab initio* density functional theory (DFT) calculations [17], hence an improved description of the system under study is needed. In this work, we present an accurate new TB model for phosphorene and PNRs calibrated on DFT simulations, and we investigate the impact of an improved bandstructure description on the electronic and transport properties of ultra-narrow PNRs, and on the operation and performance of PNR FETs at the "3 nm" CMOS technology node.

II. METHODOLOGY

Our approach employs DFT simulations for the development of a new DFT-based TB Hamiltonian model (DFT-TB), and afterwards this model is employed for NEGF device simulations. The DFT simulations are done using the OpenMX package [18], [19], employing generalized gradient approximation (GGA) with Perdew-Burke-Ernzerhof (PBE) exchange-correlation (XC) functional. The new DFT-TB model for phosphorene is developed using TBStudio [20], a software package that implements the Slater-Koster (SK) method [21]. In the new TB model, for each phosphorus atom we include 4 orbitals (s , p_x , p_y and p_z) and all relevant SK hopping integrals are accounted for ($ss\sigma$, $sp\sigma$, $pp\sigma$, $pp\pi$). Figure 1 shows the comparison of phosphorene bandstructures obtained with DFT and DFT-TB model, and clearly the new DFT-TB model achieves excellent agreement with DFT bandstructure in the energy range of interest. The SK parameters for the DFT-TB model obtained by fitting are listed in Table I.

Quantum transport based on the NEGF formalism is employed to find geometry-dependent properties such as density of states (DOS) and transmission [22], [23]. We assume ideal contacts, i.e. source/drain (S/D) extensions or reservoirs are semi-infinite semiconducting PNRs. Therefore, contact and channel regions have an identical crystal and band structure, which eliminates noncoherent effects at the interfaces and does not introduce additional contact resistance [24]. The surface Green's functions and S/D contact self-energy matrices are obtained by the Sancho-Rubio method [25]. The PNR FET I - V characteristics and related device metrics are obtained with the top-of-the-barrier (ToB) model that self-consistently solves

This work was supported by the Croatian Science Foundation under the project CONAN2D (Grant No. UIP-2019-04-3493).

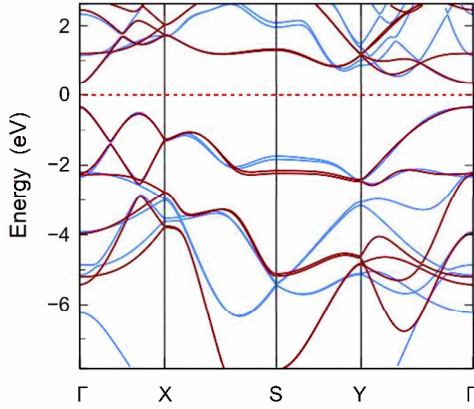


Fig. 1. Comparison of the bandstructure from DFT calculations (blue lines) and from the DFT-TB model (dark red lines). Fermi level is positioned at 0 eV (red dashed line).

Table I. On-site energies and SK parameters of the new DFT-TB model. All parameters are in eV. Bond designations are those from the TBStudio package.

On-site energies			
s	p_x	p_y	p_z
-14.168027	-3.028643	-2.618793	0.022100
Slater-Koster parameters			
Type	Bond 1	Bond 2	Bond 3
$ss\sigma$	-2.139167	3.194586	-0.737496
$sp\sigma$	-4.537056	-0.282688	-0.426628
$pp\sigma$	3.126358	3.135120	0.935184
$pp\pi$	-1.083244	-0.999519	-0.127240
Type	Bond 4	Bond 5	
$ss\sigma$	1.499989	-0.652033	
$sp\sigma$	0.581242	-0.780700	
$pp\sigma$	0.158343	1.324892	
$pp\pi$	-0.095074	-0.111658	

electrostatics coupled to NEGF DOS and transmission and provides ballistic device characteristics [16], [26], [27]. We study the performance of 15 nm-gate-length PNR FETs, for which we assume a gate oxide with EOT = 1 nm and S/D doping of 0.001 (molar fraction of the areal density of P atoms). We set a common threshold voltage (V_{TH}) of 0.24 V for all devices, as stated in the International Roadmap for Devices and Systems (IRDS) at the "3 nm" CMOS node [28], to provide a meaningful comparison between PNR FETs with different nanoribbon widths (W). Material and device simulation results we obtain using the new DFT-TB model are compared to those obtained with a simpler widely-used TB model from the literature [13].

III. RESULTS AND DISCUSSION

Figures 2 and 3 show the dispersion for 2.45 nm and 0.49 nm-wide armchair PNRs, respectively. While the literature TB model results in a symmetric single valley for both electrons and holes in the conduction and valence bands, respectively, our new DFT-TB Hamiltonian provides multi-valley dispersion characteristics in both the conduction and valence bands. Moreover, asymmetry between valence and conduction bands is obtained by the new DFT-TB model, which agrees with DFT bandstructure studies of PNRs reported in [7], [17]. With the

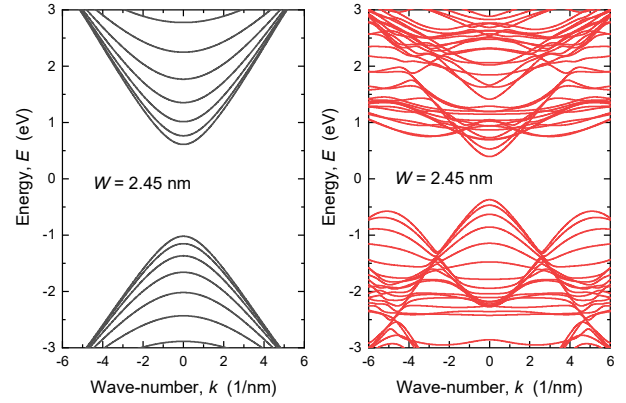


Fig. 2. Dispersion of 2.45 nm-wide PNRs with (a) TB model from the literature and (b) DFT-TB model developed in this work.

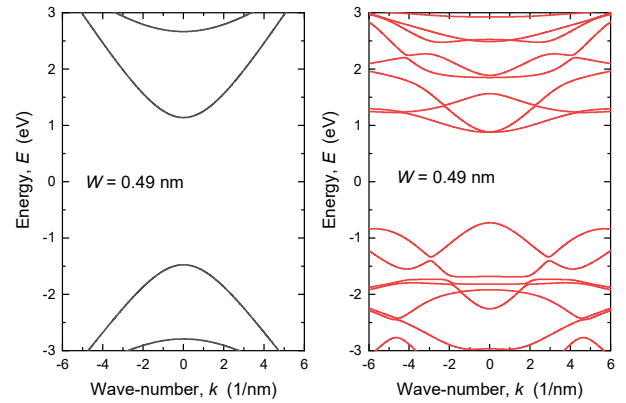


Fig. 3. Dispersion of 0.49 nm-wide PNRs with (a) TB model from the literature and (b) DFT-TB model developed in this work.

downscaling the PNR width, bandgap increases, number of subbands or conducting modes decreases, while carrier effective masses increase as can be seen from the decrease of the bottom-band curvature in Fig. 3b in comparison to Fig. 2b.

The differences and effects observed in dispersion curves consequently impact the DOS and transmission significantly. For example, Fig. 4 shows the comparison of the transmission calculated using the literature TB model and the new DFT-TB model for the PNR with $W=2.45$ nm. The difference in bandgaps comes from different XC functionals used in DFT simulations, i.e. PBE is used for our DFT-TB Hamiltonian model development, while HSE was employed for the TB model reported previously [13]. In addition, the literature TB model reproduces the transmission well only near the conduction band minimum (CBM) or valence band maximum (VBM). At higher energies, e.g. $E > \text{CBM} + 0.3$ eV, the new DFT-TB model provides a much richer transmission characteristic since more conducting modes are accounted for, which results in up to $\sim 4\times$ higher transmission in comparison to the literature TB model.

Due to significant differences in material properties resulting from using two different TB model, considerable differences are also expected in ToB FET device simulation results. This

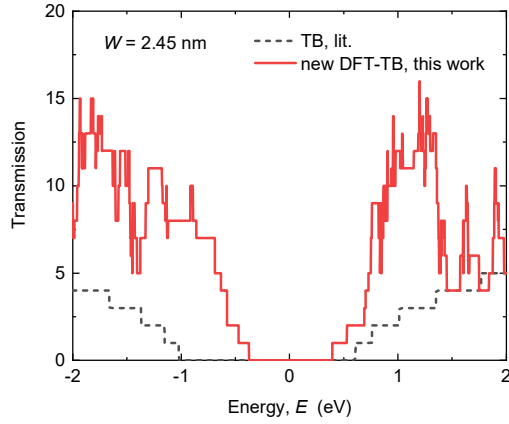


Fig. 4. Transmission for 2.45 nm-wide PNRs obtained with the two TB models. Bandgap difference comes from using different XC functionals in DFT calculations.

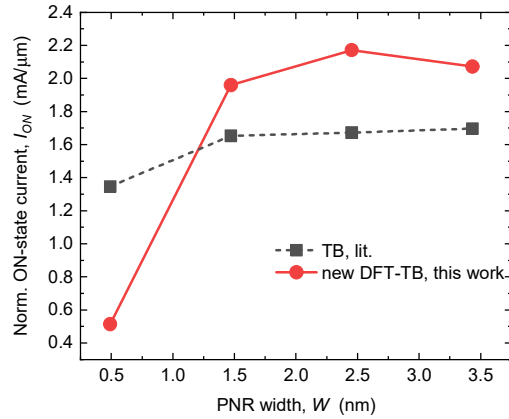


Fig. 5. Normalized I_{ON} vs. PNR width in PNR FETs calculated using the two TB models.

expectation is confirmed in Fig. 5 that reports the impact of PNR width downscaling on the width-normalized ON-state current (I_{ON}) extracted at $V_{GS} = V_{DS} = 0.7$ V. The supply voltage of 0.7 V is chosen in accordance with IRDS. Comparison between different devices and models is made meaningful by automatically adjusting the gate work function for each device so that a common $V_{TH} = 0.24$ V and a common OFF-state current of ~ 1 nA/ μm is obtained for all devices.

In the case of the literature TB model, I_{ON} is only weakly modulated by width downscaling. The maximum I_{ON} is 1.7 mA/ μm in the widest PNR FET ($W \sim 3.5$ nm) and none of the examined devices fulfills the IRDS requirement on the ON-state current at the "3 nm" node (> 1.9 mA/ μm [28]). On the other hand, using the new DFT-TB Hamiltonian models leads to qualitative and quantitative differences in the I_{ON} vs. W characteristic. The I_{ON} decreases significantly, down to ~ 0.5 mA/ μm , in the narrowest PNR device ($W \sim 0.5$ nm) when a more accurate bandstructure is considered in FET simulations. The difference between the two models for $W = 0.5$ nm equals $\sim 2.7\times$, which demonstrates that the simpler TB model underestimates the severity of bandstructure effects in the narrowest PNR. However, the trend is opposite for wider PNRs because we observe a much higher I_{ON} for $W > 1.2$ nm for the

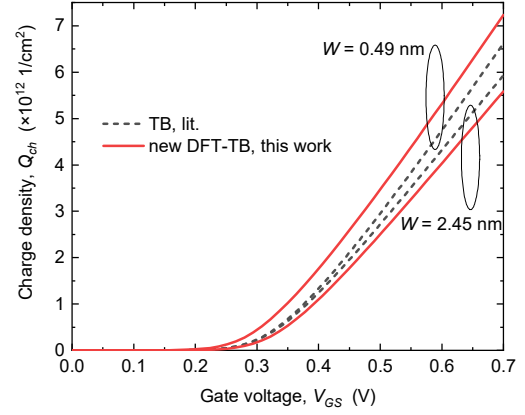


Fig. 6. Comparison of gate-voltage-dependent charge density for the two models in PNR FETs with 2.45 nm and 0.49 nm-wide PNRs.

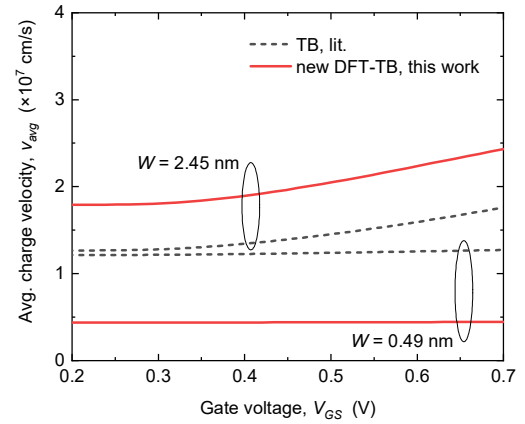


Fig. 7. Comparison of gate-voltage-dependent average charge velocity for the two models in PNR FETs with 2.45 nm and 0.49 nm-wide PNRs.

DFT-TB model than for the literature TB model. The maximum I_{ON} reaches ~ 2.2 mA/ μm in the ~ 2.5 nm-wide PNR FET. In contrast to the literature TB model, the improved bandstructure description enabled by our new DFT-TB model reveals that PNR FETs with $W > 1.4$ nm and with negligible scattering can meet IRDS I_{ON} goal at the "3 nm" node.

The differences between the two models and related bandstructure effects on the device performance can be more readily understood by exploring the channel charge density (Q_{ch}), shown in Fig. 6, and average charge velocity (v_{avg}), reported in Fig. 7. Both figures contain gate voltage dependent characteristics for the 0.49 nm and 2.45 nm-wide PNRs. For both devices and models in Fig. 6, the Q_{ch} increases with V_{GS} as expected. The new DFT-TB model results in a higher (lower) carrier density in the narrower (wider) PNR, and all curves are relatively closely spaced. However, differences in v_{avg} are considerable, and they are the dominant factor that causes the difference in I_{ON} behavior reported in Fig. 5. Namely, when the new DFT-TB model is used, the 2.45 nm-wide PNR has a lower effective electron mass (see the dispersion around the CBM in Fig. 2) and thus a higher v_{avg} (as shown in Fig. 7). On the other hand, using the DFT-TB Hamiltonian for the 0.49 nm-wide PNR results in heavier carriers than in the case of the simpler

literature TB model (Fig. 3). Therefore, better (worse) current driving capabilities of n -channel PNR FETs with $W > 1.2$ nm ($W < 1.2$ nm) are mainly attributed to the electron effective mass modification by the geometry-dependent bandstructure effects.

We note that in realistic devices several intrinsic and extrinsic scattering mechanisms would deteriorate the transport properties and reduce the current driving capabilities [29]. In addition, parasitic contact resistance is neglected in this work, which is known to significantly impact the performance of nanoribbon FETs [12], [16], [30]. However, our work illustrated the importance of using a proper TB Hamiltonian in the simulation of PNR devices, with a considerable improvement of PNR FET figures-of-merit in comparison to a simple TB model.

IV. CONCLUSION

We report a new DFT-based TB model for the atomistic quantum transport simulations of phosphorene-based nanodevices. This new model reproduces the complex bandstructure (multi-valley dispersion, and valence and conduction band asymmetry) of PNRs and allows more accurate but still numerically efficient device simulations. We demonstrate significant differences between the two TB models in terms of electronic and transport properties, including transmission, free carrier density, average carrier velocity in the channel, and PNR FET device performance. In contrast to the literature TB model, using an improved bandstructure description with the new DFT-TB model reveals that ballistic PNR FETs with $W > 1.4$ nm can meet IRDS requirement for I_{ON} at the "3 nm" CMOS technology node.

REFERENCES

- [1] K. S. Novoselov *et al.*, "Electric Field Effect in Atomically Thin Carbon Films," *Science*, vol. 306, no. 5696, pp. 666–669, Oct. 2004, doi: 10.1126/science.1102896.
- [2] H. Liu *et al.*, "Phosphorene: An Unexplored 2D Semiconductor with a High Hole Mobility," *ACS Nano*, vol. 8, no. 4, pp. 4033–4041, Apr. 2014, doi: 10.1021/nn501226z.
- [3] S. Das, M. Demarteau, and A. Roelofs, "Ambipolar Phosphorene Field Effect Transistor," *ACS Nano*, vol. 8, no. 11, pp. 11730–11738, Nov. 2014, doi: 10.1021/nn505868h.
- [4] C. Klinkert, Á. Szabó, C. Stieger, D. Campi, N. Marzari, and M. Luisier, "2-D Materials for Ultrascaled Field-Effect Transistors: One Hundred Candidates under the Ab Initio Microscope," *ACS Nano*, vol. 14, no. 7, pp. 8605–8615, Jul. 2020, doi: 10.1021/acsnano.0c02983.
- [5] L. Li *et al.*, "Black phosphorus field-effect transistors," *Nat. Nanotechnol.*, vol. 9, no. 5, pp. 372–377, May 2014, doi: 10.1038/nnano.2014.35.
- [6] N. Haratipour, M. C. Robbins, and S. J. Koester, "Black Phosphorus p-MOSFETs With 7-nm HfO₂ Gate Dielectric and Low Contact Resistance," *IEEE Electron Dev. Lett.*, vol. 36, no. 4, pp. 411–413, Apr. 2015, doi: 10.1109/LED.2015.2407195.
- [7] A. Carvalho, A. S. Rodin, and A. H. C. Neto, "Phosphorene nanoribbons," *Europhys. Lett.*, vol. 108, no. 4, p. 47005, Nov. 2014, doi: 10.1209/0295-5075/108/47005.
- [8] H. Guo, N. Lu, J. Dai, X. Wu, and X. C. Zeng, "Phosphorene Nanoribbons, Phosphorus Nanotubes, and van der Waals Multilayers," *J. Phys. Chem. C*, vol. 118, no. 25, pp. 14051–14059, Jun. 2014, doi: 10.1021/jp505257g.
- [9] M. C. Watts *et al.*, "Production of phosphorene nanoribbons," *Nature*, vol. 568, no. 7751, pp. 216–220, Apr. 2019, doi: 10.1038/s41586-019-1074-x.
- [10] X. Han, H. Morgan Stewart, S. A. Shevlin, C. R. A. Catlow, and Z. X. Guo, "Strain and Orientation Modulated Bandgaps and Effective Masses of Phosphorene Nanoribbons," *Nano Lett.*, vol. 14, no. 8, pp. 4607–4614, Aug. 2014, doi: 10.1021/nl501658d.
- [11] M. Poljak, "Electron Mobility in Defective Nanoribbons of Monoelemental 2D Materials," *IEEE Electron Dev. Lett.*, vol. 41, no. 1, pp. 151–154, Jan. 2020, doi: 10.1109/LED.2019.2952661.
- [12] M. Poljak and M. Matic, "Quantum Transport Simulations of Phosphorene Nanoribbon MOSFETs: Effects of Metal Contacts, Ballisticity and Series Resistance," in *2020 International Conference on Simulation of Semiconductor Processes and Devices (SISPAD)*, Sep. 2020, pp. 371–374, doi: 10.23919/SISPAD49475.2020.9241601.
- [13] A. N. Rudenko and M. I. Katsnelson, "Quasiparticle band structure and tight-binding model for single- and bilayer black phosphorus," *Phys. Rev. B*, vol. 89, no. 20, p. 201408, May 2014, doi: 10.1103/PhysRevB.89.201408.
- [14] D. Yin and Y. Yoon, "Design strategy of two-dimensional material field-effect transistors: Engineering the number of layers in phosphorene FETs," *J. Appl. Phys.*, vol. 119, no. 21, p. 214312, Jun. 2016, doi: 10.1063/1.4953256.
- [15] M. Poljak and T. Suligoj, "Immunity of electronic and transport properties of phosphorene nanoribbons to edge defects," *Nano Res.*, vol. 9, no. 6, pp. 1723–1734, Jun. 2016, doi: 10.1007/s12274-016-1066-1.
- [16] M. Poljak, M. Matic, and A. Zeljko, "Minimum Contact Resistance in Monoelemental 2D Material Nanodevices with Edge-Contacts," *IEEE Electron Dev. Lett.*, 2021, (in press) doi: 10.1109/LED.2021.3087908.
- [17] L. Liang, J. Wang, W. Lin, B. G. Sumpter, V. Meunier, and M. Pan, "Electronic Bandgap and Edge Reconstruction in Phosphorene Materials," *Nano Lett.*, vol. 14, no. 11, pp. 6400–6406, Nov. 2014, doi: 10.1021/nl502892t.
- [18] T. Ozaki, "Variationally optimized atomic orbitals for large-scale electronic structures," *Phys. Rev. B*, vol. 67, no. 15, p. 155108, Apr. 2003, doi: 10.1103/PhysRevB.67.155108.
- [19] "OpenMX website." <http://www.openmx-square.org/>
- [20] M. Nakhaee, S. A. Ketabi, and F. M. Peeters, "Tight-Binding Studio: A technical software package to find the parameters of tight-binding Hamiltonian," *Computer Physics Communications*, vol. 254, p. 107379, Sep. 2020, doi: 10.1016/j.cpc.2020.107379.
- [21] J. C. Slater and G. F. Koster, "Simplified LCAO Method for the Periodic Potential Problem," *Phys. Rev.*, vol. 94, no. 6, pp. 1498–1524, Jun. 1954, doi: 10.1103/PhysRev.94.1498.
- [22] S. Datta, *Quantum Transport: Atom to Transistor*, 2nd ed. New York, NY, USA: Cambridge University Press, 2005.
- [23] M. Luisier, "Quantum transport beyond the effective mass approximation," Doctoral Thesis, ETH Zurich, 2007. doi: 10.3929/ethz-a-005340630.
- [24] M. Poljak and M. Matic, "Metallization-Induced Quantum Limits of Contact Resistance in Graphene Nanoribbons with One-Dimensional Contacts," *Materials*, vol. 14, no. 13, p. 3670, Jan. 2021, doi: 10.3390/ma14133670.
- [25] M. P. L. Sancho, J. M. L. Sancho, J. M. L. Sancho, and J. Rubio, "Highly convergent schemes for the calculation of bulk and surface Green functions," *J. Phys. F: Met. Phys.*, vol. 15, no. 4, p. 851, 1985, doi: 10.1088/0305-4608/15/4/009.
- [26] A. Rahman, Jing Guo, S. Datta, and M. S. Lundstrom, "Theory of ballistic nanotransistors," *IEEE Trans. Electron Devices*, vol. 50, no. 9, pp. 1853–1864, Sep. 2003, doi: 10.1109/TED.2003.815366.
- [27] S. Kaneko, H. Tsuchiya, Y. Kamakura, N. Mori, and M. Ogawa, "Theoretical performance estimation of silicene, germanene, and graphene nanoribbon field-effect transistors under ballistic transport," *Appl. Phys. Express*, vol. 7, no. 3, p. 035102, Mar. 2014, doi: 10.7567/APEX.7.035102.
- [28] "IEEE International Roadmap for Devices and Systems (IRDS), 2019 Update." <https://irds.ieee.org/>
- [29] G. Gaddemane, M. L. Van de Put, W. G. Vandenberghe, E. Chen, and M. V. Fischetti, "Monte Carlo analysis of phosphorene nanotransistors," *J. Comput. Electron.*, Jan. 2021, doi: 10.1007/s10825-020-01610-6.
- [30] M. Poljak, "Impact of Width Scaling and Parasitic Series Resistance on the Performance of Silicene Nanoribbon MOSFETs," *IEEE Trans. Electron Devices*, vol. 67, no. 11, pp. 4705–4708, Nov. 2020, doi: 10.1109/TED.2020.3017465.